Adaptive Shape Functions and Internal Mesh Adaptation for Modelling Progressive Failure in Adhesively Bonded Joints

Scott E. Stapleton and Thomas Gries
RWTH Aachen University, Aachen, Deutschland

Anthony M. Waas
University of Michigan, Ann Arbor, Michigan

Evan J. Pineda
Glenn Research Center, Cleveland, Ohio

NASA STI Program . . . in Profile

Since its founding, NASA has been dedicated to the advancement of aeronautics and space science. The NASA Scientific and Technical Information (STI) program plays a key part in helping NASA maintain this important role.

The NASA STI Program operates under the auspices of the Agency Chief Information Officer. It collects, organizes, provides for archiving, and disseminates NASA's STI. The NASA STI program provides access to the NASA Aeronautics and Space Database and its public interface, the NASA Technical Reports Server, thus providing one of the largest collections of aeronautical and space science STI in the world. Results are published in both non-NASA channels and by NASA in the NASA STI Report Series, which includes the following report types:

- TECHNICAL PUBLICATION. Reports of completed research or a major significant phase of research that present the results of NASA programs and include extensive data or theoretical analysis. Includes compilations of significant scientific and technical data and information deemed to be of continuing reference value. NASA counterpart of peer-reviewed formal professional papers but has less stringent limitations on manuscript length and extent of graphic presentations.

- TECHNICAL MEMORANDUM. Scientific and technical findings that are preliminary or of specialized interest, e.g., quick release reports, working papers, and bibliographies that contain minimal annotation. Does not contain extensive analysis.

- CONTRACTOR REPORT. Scientific and technical findings by NASA-sponsored contractors and grantees.

- CONFERENCE PUBLICATION. Collected papers from scientific and technical conferences, symposia, seminars, or other meetings sponsored or cosponsored by NASA.

- SPECIAL PUBLICATION. Scientific, technical, or historical information from NASA programs, projects, and missions, often concerned with subjects having substantial public interest.

- TECHNICAL TRANSLATION. English-language translations of foreign scientific and technical material pertinent to NASA's mission.

Specialized services also include creating custom thesauri, building customized databases, organizing and publishing research results.

For more information about the NASA STI program, see the following:

- Access the NASA STI program home page at *http://www.sti.nasa.gov*

- E-mail your question to *help@sti.nasa.gov*

- Fax your question to the NASA STI Information Desk at 443–757–5803

- Phone the NASA STI Information Desk at 443–757–5802

- Write to:
  STI Information Desk
  NASA Center for AeroSpace Information
  7115 Standard Drive
  Hanover, MD 21076–1320

Adaptive Shape Functions and Internal Mesh Adaptation for Modelling Progressive Failure in Adhesively Bonded Joints

Scott E. Stapleton and Thomas Gries
RWTH Aachen University, Aachen, Deutschland

Anthony M. Waas
University of Michigan, Ann Arbor, Michigan

Evan J. Pineda
Glenn Research Center, Cleveland, Ohio

Acknowledgments

Level of Review: This material has been technically reviewed by technical management.

Available from

NASA Center for Aerospace Information
7115 Standard Drive
Hanover, MD 21076–1320

National Technical Information Service
5301 Shawnee Road
Alexandria, VA 22312

Available electronically at http://www.sti.nasa.gov

Adaptive Shape Functions and Internal Mesh Adaptation for Modelling Progressive Failure in Adhesively Bonded Joints

Scott E. Stapleton and Thomas Gries
RWTH Aachen University
Aachen, Deutschland 52074

Anthony M. Waas
University of Michigan
Ann Arbor, Michigan 48105

Evan J. Pineda
National Aeronautics and Space Administration
Glenn Research Center
Cleveland, Ohio 44135

Abstract

Enhanced finite elements are elements with an embedded analytical solution that can capture detailed local fields, enabling more efficient, mesh independent finite element analysis. The shape functions are determined based on the analytical model rather than prescribed. This method was applied to adhesively bonded joints to model joint behavior with one element through the thickness. This study demonstrates two methods of maintaining the fidelity of such elements during adhesive non-linearity and cracking without increasing the mesh needed for an accurate solution. The first method uses adaptive shape functions, where the shape functions are recalculated at each load step based on the softening of the adhesive. The second method is internal mesh adaption, where cracking of the adhesive within an element is captured by further discretizing the element internally to represent the partially cracked geometry. By keeping mesh adaptations within an element, a finer mesh can be used during the analysis without affecting the global finite element model mesh. Examples are shown which highlight when each method is most effective in reducing the number of elements needed to capture adhesive nonlinearity and cracking. These methods are validated against analogous finite element models utilizing cohesive zone elements.

Introduction

With the increasing demand for fiber reinforced composites in lightweight aerospace structures, adhesively bonded joints are becoming more critical than ever. Bolted and riveted joints have proven to be poorly suited for composite materials (Ref. 1). Unlike traditional metals, brittle fibers often do not yield significantly to spread concentrated loads introduced by mechanical fasteners. Furthermore, bolts and rivets require holes in the material to be joined, which interrupts continuous fibers and introduces additional stress concentrations. Adhesive bonding is suitable for composite materials because it is less invasive, introduces load more gradually, and can often be much more cost effective. The adhesive market has indeed grown along with the advanced composite market, and the structural adhesive market in Europe has been forecasted to reach 67,000 tons by 2015; a growth of over 13 percent since 2008 (Ref. 2).

However, adhesively bonded joints can be problematic to model. The models often do not scale because of fixed thickness requirements of the adhesive layers, making individual design for each joint necessary. Geometric discontinuities in adherends cause stress singularities in many models, thus non-traditional failure criteria or evaluation methods are often required. A lack of confidence in material models, failure criteria, and engineering experience results in gross over-design of joints along with safety requirements which sometimes require secondary mechanical fasteners, jokingly referred to as "chicken bolts" by many engineers.

Adhesively bonded joints are typically analyzed using analytical models (closed-form) or numerical models (finite elements). Historically, analytical models (Refs. 3 to 12) were relied upon exclusively while computer capability was relatively small. Analytical models are fast, and have been used to conduct numerous parametric studies to further the understanding of the design of joints. However, assumptions are often made which allow closed-form solutions but limit joint geometry and materials which can be accurately analyzed. Furthermore, these analytical models do not couple well with larger component and vehicle models, limiting their usefulness.

Finite element (FE) models, on the other hand, are general enough to allow a wide range of geometries and configurations, and can even couple joint analysis with larger models. The improving speed of computers makes this method more viable for joint analysis. However, there are some downsides to modeling joints with FE models. The reentrant corners often cause a geometric singularity, and numerous work has been conducted to create failure theories which account for this (Refs. 13 to 19). Failure methods investigated include stress-based, strain based, plastic energy density, and stress measured at a characteristic distance from the singularity. Furthermore, the extremely thin adhesive layer limits the size of elements which can be used to explicitly model the adhesive. This means that there are truly no coarse models, and coupling with vehicle-scale models can be problematic (Refs. 15 and 16).

One relatively new technique for modeling progressive failure of adhesively bonded joints is progressive damage modeling incorporating fracture mechanics concepts. Interface elements using different methods such as discrete cohesive zone method (DCZM) or continuous cohesive zone method (CCZMare) used to resolve the stress singularity at material interfaces and reentrant geometrical corners, and allow the faces of the adherends to separate by treating the adhesive as a network of non-linear springs obeying a traction versus separation law (Refs. 20 to 26). These methods come in many different varieties, but most often involve stress-based initiation criterion and energy-based failure definitions. These methods have been shown to be extremely powerful for joints, but still have some drawbacks. Characterizing these interface elements requires a large amount of characterization tests, and appropriate handling of mode-mixity is also a subject within the cohesive zone modeling that has yet to be satisfactorily concluded (Ref. 25). Additionally, the cohesive laws utilized require an initial, numerical fictitious stiffness to prevent separation of the plies before delamination initiation. Furthermore, there is a maximum element length, based on the process zone size, required to obtain accurate results. Cohesive zone element utilizing shape functions that are enriched by an analytical solution (similar to the methodology presented in this work) have been used to alleviate mesh dependence and size requirements (Refs. 25 and 26). Most cohesive elements are formulated assuming a zero-thickness interface, and thus may not be adequate to model adhesive joints, especially if the adhesive layer is thick.

Another fracture based technique for modeling crack propagation that can be applied to joint analysis is the virtual crack closure technique (VCCT) [KRUEGER, 2004]. With VCCT fracture toughness based criteria are used to determine if it is energetically favorable for a crack to propagate. Propagation is restricted to element boundaries and typically must be known *a priori*. Thus, modeling joints with a finite thickness adhesive may prove challenging with VCCT.

All of the aforementioned methods are highly developed and have been shown to give a reasonable strength prediction for joints, but they are detailed models which require extremely fine meshes. Thin adhesive bonds, most often thinner than 1 mm, restrict the size of elements needed for the adhesive. The transition from the fine adhesive mesh to the coarser adherend mesh causes additional preprocessing work for the analyst. Therefore, joint design and analysis is typically completed after the global vehicle sizing on dense meshed sub-models, when design changes are expensive or impractical.

A need exists to develop predictive tools for bonded joints that can be seamlessly coupled with large scale structural analyses without adding major computational demands. Such tools can be used to make quick mesh-independent assessments of bonded composite joints. Furthermore, they fit in into the computational hierarchy of virtual testing of aircraft structures (Ref. 27), an area that is getting increased attention in the aerospace industry with the aim of lowering design cycle and certification costs.

A solution to this problem involves merging analytical models with finite elements. Simplified structural models can be used to obtain shape functions that are exact for the assumptions of the model. These shape functions can be used to formulate stiffness matrix for the problem at hand. As long as the assumptions remain valid, such an element would give the exact solution regardless of the number of elements used.

This method has been used to calculate an stiffness matrix for different beam on elastic foundation problems (Refs. 28 and 29). More recently, Waas and Gustafson (Ref. 30) have created an element to capture the behavior of a double overlap joint subjected to mechanical and thermal loads.

A general bonded joint finite element has been created (Refs. 30 to 33) wherein an entire bonded joint can be modeled with a single element. This joint element considers the adherends to behave like beams (or wide panels), and the adhesive to be made up of a bed of shear and normal nonlinear springs. The governing equations of this structural model are found and solved to produce enhanced shape functions for the joint element. Furthermore, the element has been generalized to allow multiple adherend/adhesive layers and ply drops/thickness tapers, providing the capability to model a variety of joint types with very few elements. This model was implemented in the software Joint Element Designer, which was written in C# and first conceived in a joint effort between the University of Michigan and NASA. However, this method loses its advantage when modeling highly nonlinear adhesives and trying to capture progressive failure. An increase in elements is required for an accurate solution, which goes against the philosophy of enhanced elements.

This paper presents two methods which allow the bonded joint finite element to capture adhesive non-linearities and cracking without increasing the mesh needed for an accurate solution. The first method is the use of adaptive shape functions, where the shape functions are recalculated at each load step based on the softening of the adhesive. The second method is internal mesh adaption, where cracking of the adhesive within an element is represented by discretizing a cracked element into multiple elements in order to accurately represent the local, cracked geometry. Both of these methods were implemented in the Joint Element Designer software. Examples are shown which highlight the savings in elements, computational time, and integration points needed when using these methods and when the methods are particularly beneficial. The performance of the various joint element methodologies are compared to analogous models using CZM elements.

Finally, while these methods are shown for an adhesively bonded joint but both methods have broader application. The adaptive shape functions could be used for any element where the material and geometric properties used to obtain the shape functions are changing. Updating the shape functions within an analysis would improve the ability of the shape functions to represent the deformation of the changing material/geometry. Finally, adaptive mesh, which is not a new technique (Refs. 25, 26, 34, and 35), can be very effective in capturing discontinuities within an element without changing the elements relationship with the global model.

Formulation

The formulation presented here is merely a summary of the formulation of the joint element, and the details presented are considered by the authors to be required for the understanding of the current study. For a more detailed formulation, the reader is encouraged to consult prior work (Ref. 36).

Consider a structure consisting of N layers of thin plates under cylindrical bending joined together by N-1 thin layers of a much more compliant adhesive material (Figure 1(a)). The plates are assumed to behave as "wide" layered composite Euler Bernoulli beams (hence the cylindrical bending assumption). The axial displacement of adherend i, u_i, varies linearly through the thickness and the transverse and rotational displacements, w_i and $w_{i,x}$, are assumed to be constant through the cross section. Additionally, it is assumed that the only significant stresses are the axial stresses induced by bending and axial deformation, so other stress components in the adherend can be neglected. The adhesive joining the plates is modeled as a Winkler foundation, where only peel and shear stress are included and the stresses are assumed to be constant though the thickness of the adhesive layer. With the displacement behavior known in the transverse, z_i, direction, the problem can be formulated in terms of one dimension, x.
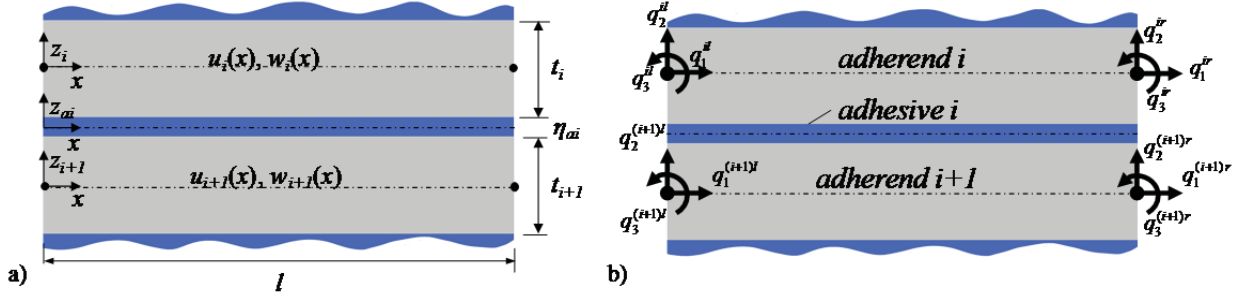
Figure 1.—Adhesively bonded joint element (a) geometric parameters and (b) finite element discretization.

Shape Functions for Linear Elastic Case

The shape functions used for the joint element were derived by analytically solving the governing equations of the linear elastic joint model (Refs. 33 and 36). Using the principle of stationarity of potential energy and the aforementioned approximations, $2N$ fully coupled governing equilibrium differential equations are obtained. Of the $2N$ governing equations, N equations correspond to the axial equilibrium, while N equations correspond to the transverse equilibrium. The axial displacement equilibrium equations contain second order derivatives, while the transverse displacement equations have fourth order derivatives. The order of these equations can be reduced and assembled into a system of first order constant coefficient homogeneous ordinary differential equations of the form

$$\mathbf{u}_{,x} = \mathbf{A}\mathbf{u} \tag{1}$$

where $\mathbf{u}$ is a vector containing the adherend centerline vectors of all of the N adherends:

$$\mathbf{u} = \begin{bmatrix} \mathbf{u}_1^T & \cdots & \mathbf{u}_i^T & \cdots & \mathbf{u}_N^T \end{bmatrix}^T \tag{2}$$

and the centerline vector of adherend i is defined as

$$\mathbf{u}_i = \begin{bmatrix} u_i(x) & u_i(x)_{,x} & w_i(x) & w_i(x)_{,x} & w_i(x)_{,xx} & w_i(x)_{,xxx} \end{bmatrix}^T \tag{3}$$

where, x denotes the derivative with respect to x. This form of defining the centerline displacements might not be conventional, but it is used to lead into our solution strategy of the governing equations. Using state variables with higher order derivatives as is done here allows the governing equations to be reduced to a series of first order differential equations.

One downside to this method worth mentioning is its dependence on solving the system of ODE's to get the shape functions. This makes the extension of this method to a plate or shell-type element difficult because such an element would require the solution of a PDE, which can be significantly more difficult and time-consuming.

The system of ordinary differential equations in Equation (1) is solved using the matrix exponential and rewritten in terms of the nodal degrees of freedom, $\mathbf{q}$ (Figure 1(b)), and shape functions, $\mathbf{N}$, in the form:

$$\mathbf{u} = \mathbf{N}\mathbf{q} \tag{4}$$

The main thing to consider is that the shape functions were not prescribed, as is normally the case in finite elements, but derived by solving the governing equations for the stacked beam model. Therefore, the shape functions are a function of the geometric and material parameters of the adherend and adhesive layers:

$$\mathbf{N} = \mathbf{N}\big((E_i, t_i, b_i)_{i=1..N}, (E_{ai}, G_{ai}, \eta_{ai}, b_{ai})_{ai=1..N-1}\big) \tag{5}$$

Material and Geometric Nonlinearities

Since modern polymeric adhesives often display highly nonlinear material behavior, it was necessary to include material nonlinearities in the joint element to estimate joint strengths more correctly. A particularly simple nonlinear elastic stress law was chosen:

$$\boldsymbol{\sigma} = \boldsymbol{\sigma}(\boldsymbol{\varepsilon}) \tag{6}$$

where the stress is some general function of the strain in the adhesive and adherends. Although it would be more correct to use an incremental flow type plasticity formulation that distinguishes loading and unloading stiffness, the simple nonlinear elastic relation, which assumes no permanent plastic strain, was chosen for several reasons. The joint element is meant to be a design tool to give general approximations, so it is not expected that such a tool will be used in situations requiring unloading capabilities. Additionally, the nature of adhesively bonded joints is such that the high stresses occur in concentrated form at the joint edges. Since the failing adhesive domain is eliminated in the iteration process (to be described later) the assumption of a nonlinear elastic type stress-strain law suffices for this modeling process since potential regions of "unloading" are minimal and contained in the regions which are eliminated. Thus, this assumption does lead to a meaningful rendition of the joint physics, yet facilitating an efficient (in the computational sense) solution strategy.

The elemental stiffness matrix, $\mathbf{k}$, is found by integrating the:

$$\mathbf{k} = \int_V \mathbf{B}^T \mathbf{D}(\mathbf{q}) \mathbf{B} dV \tag{7}$$

where $\mathbf{B}$ is the matrix linking the strains and nodal degrees of freedom (which contains the shape functions for the initial linearly elastic state: $\mathbf{N}$), and $\mathbf{D}(\mathbf{q})$ is the nonlinear tangent stiffness matrix.

Additionally, a co-rotational formulation was used to account for large rotations in the system, as described in References 37 to 39 and adapted to the joint element in Reference 36.

Adaptive Shape Functions

When the adhesive in a joint element has a nonlinear stress-strain relationship, the shape functions obtained for a linearly elastic adhesive may no longer be well-suited. The shape functions were derived based on a solution of the governing equations of the problem, so the stiffness of the materials is used to acquire the shape functions. As the adhesive softens, the tangent modulus changes and the shape functions found before loading no longer represent the solution of the governing equations based on the softened adhesive tangent modulus. This is illustrated in Figure 2, where a joint with a highly ductile adhesive is loaded and the shape functions (Figure 2(d)) are required to change as the adhesive softens. For highly nonlinear materials, many elements may be required to accurately capture the joint behavior.
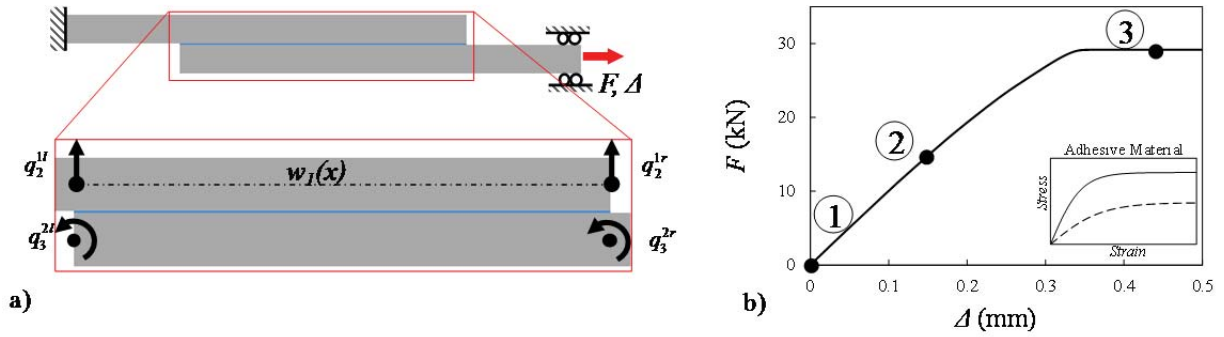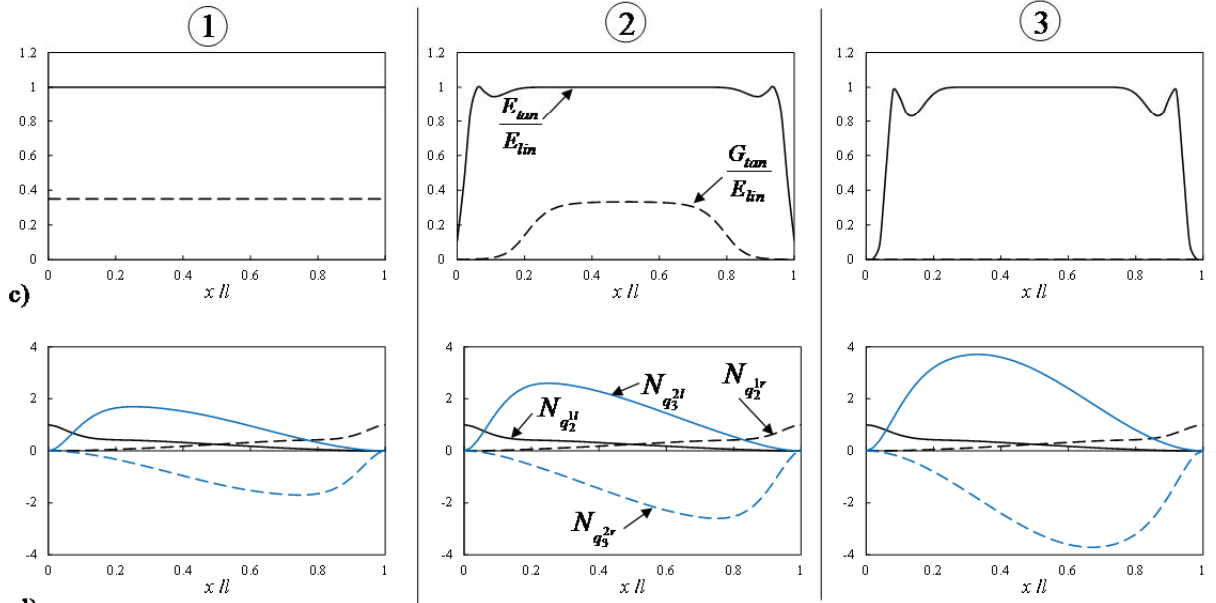
Figure 2.—Demonstration of shape function progression during a loading scenario: (a) single lap joint under tension, (b) load versus displacement highlighting three points, and (c) tangent modulus of the adhesive and (d) selected shape functions at each of the three points.

To address this issue, adaptive shape functions were applied to the joint element. After each load increment, the shape functions for the next increment are calculated for a joint where the stiffness of the joint changes along the *x*-direction. The function for the adhesive modulus, $E_{ai}(x)$, is based on the tangent stiffness of the adhesive in the prior load increment. The peel stress in adhesive *i* can be written in terms of the peel strain as

$$\sigma_{a_i} = E_{a_i}(x)\varepsilon_{a_i} \tag{8}$$

and similarly for the shear stress:

$$\tau_{a_i} = G_{a_i}(x)\gamma_{a_i} \tag{9}$$
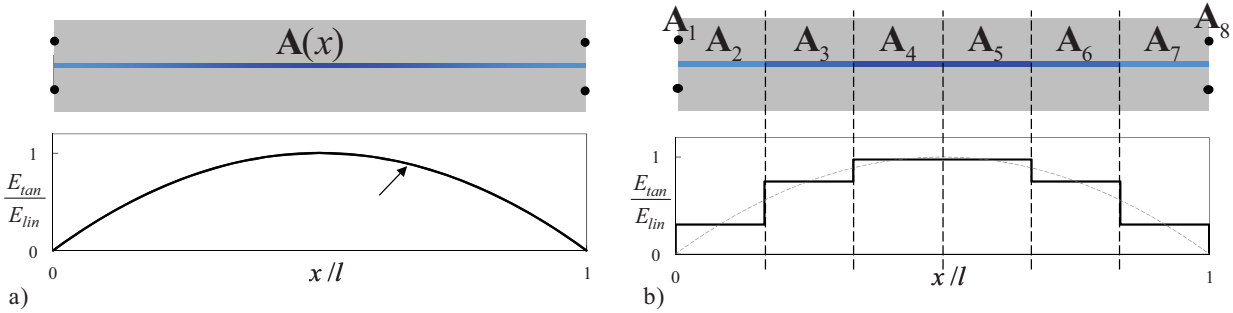
Figure 3.—To solve the governing equations for (a) an element with a softened adhesive, the joint element was (b) discretized into regions (in this case 6) within which the tangent modulus was considered constant.

This causes the system of governing equations to now have non-constant coefficients (compare with Eq. (1))

$$\mathbf{u}_{,x} = \mathbf{A}(x)\mathbf{u} \tag{10}$$

where the coefficient matrix, $\mathbf{A}(x)$, is now a function of x. Since the coefficient matrix is non-constant, a semi-numerical method of solution was adopted. The domain was split into segments in which the coefficient matrix, $\mathbf{A}(x)$, was considered constant and solved using the matrix exponential for that section (Figure 3). The sections were than linked together with boundary conditions, and an approximate solution of $\mathbf{A}(x)$ was found (Ref. 32).

The number of segments was determined by the number of integration points, so that the shape functions were refined with an increasing number of integration points. It should be acknowledged that the discretization involved in this method is very similar to conventional finite element discretization. This may serve to reduce the advantages of using the joint element, but it still allows for the joint to be represented with very few elements, simplifying analysis steps like mesh generation and post-processing.

The shape functions were re-calculated at each loading step in the analysis. This adds to the computational time, but can be extremely advantageous in reducing the required mesh for highly non-linear adhesives.

Crack Growth

When some user-defined failure criterion is reached in some part of the adhesive layer, that portion of the adhesive is considered "failed" and can carry no load and has no stiffness. Setting the stress and stiffness of that portion of the adhesive to zero is an easy way to model the failure of the adhesive, but the shape functions for the joint element were not originally calculated based on a joint with failed adhesive, and cannot accurately model this new situation. Therefore, as with traditional finite elements, more elements are required to accurately find the solution where the adhesive has failed. In the case of failed adhesive, a great number of elements may be needed, as will be illustrated later.

In order to increase the accuracy of the joint element after adhesive failure and crack growth, a method of removing the adhesive and adapting the mesh to the crack was devised. Since the joint element is meant to be used as a user-defined element in a larger global assembly in commercially available finite element software, the mesh change would have to be strictly internal to the element so that the surrounding model does not have to change. Therefore, a sub-assembly method was devised to handle adhesive failure as shown in Figure 4 and outlined in Figure 5.
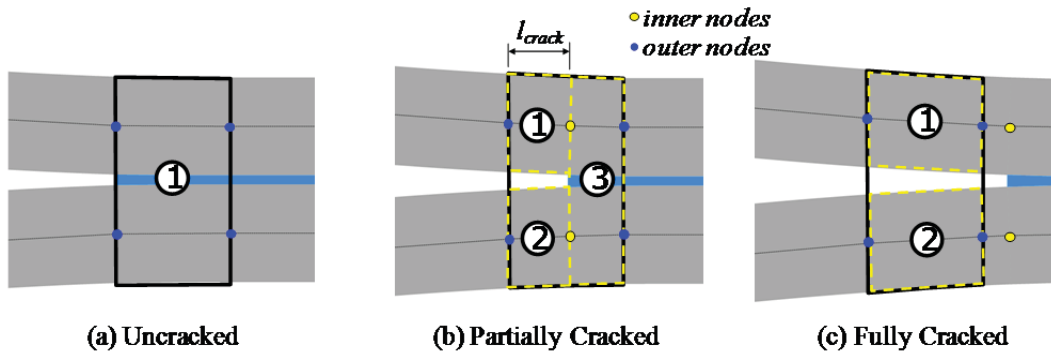
Figure 4.—Diagram showing (a) an uncracked joint element, (b) a partially cracked element, and (c) a fully cracked joint element, and the addition of internal sub-elements.
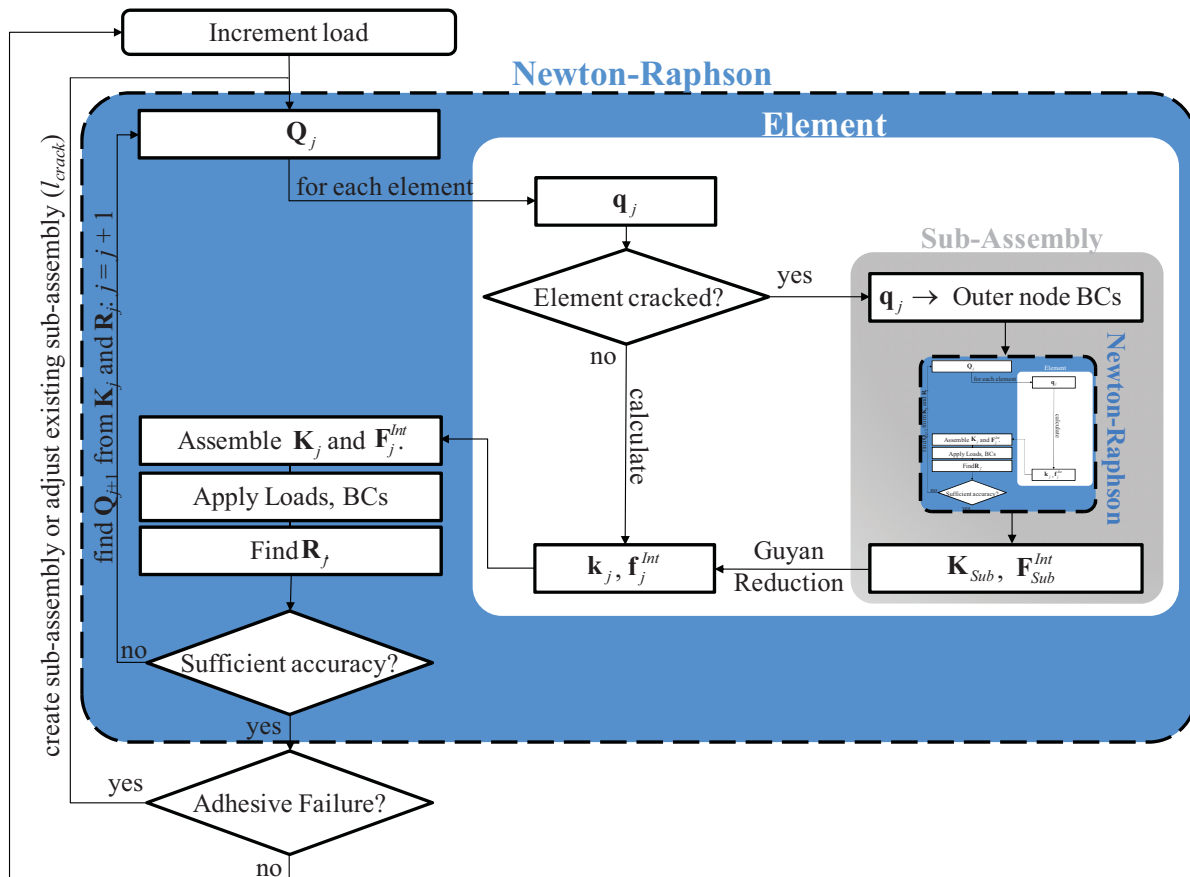
Figure 5.—Flow chart showing how cracked element sub-assembly is incorporated into joint element solution procedure.

As with standard finite element analysis, a Newton-Raphson type solver is used to solve the global system of equations. At load increment j, the global degrees of freedom (dofs), $\mathbf{Q}_j$, are guessed, and this is broken down into elemental dofs, $\mathbf{q}_j$. After applying the prescribed displacements to the joint element, the adhesive is checked for failure or cracking.

If failure in the adhesive is detected, the element is replaced by a sub-assembly with three elements as shown in Figure 4(b). The length of the crack, $l_{crack,}$ determines the lengths of the sub-assembly elements. The displacement of the inner nodes is unknown, therefore the sub-assembly becomes a nonlinear model within another nonlinear model and must be solved with its own Newton-Raphson type solution

procedure. A sub-assembly Newton-Raphson type solver is employed, the elemental dof are used as outer node boundary conditions, and the stiffness, $\mathbf{K}_{Sub}$, and internal force vector, $\mathbf{F}_{Sub}^{Int}$, for the sub-assembly are calculated. However, these quantities still have the inner degrees of freedom contained within. The force vector and stiffness matrix are then reduced using the Guyan Reduction Method (Refs. 40 to 42). Once the internal degrees of freedom are removed, the stiffness matrix and force vector, $\mathbf{k}_j$ and $\mathbf{f}_j^{Int}$, can be considered to be that of the equivalent joint element, and are passed on to the global assembly.

These vectors/matrices for all of the elements in the assembly are assembled, boundary conditions and loads are applied, and the residual, $\mathbf{R}_j$, (error of the initial nodal displacement guess) is calculated. If the residual is not within some tolerated state, a new nodal displacement "guess" is calculated based on the previous displacement, residual, and stiffness values and the whole cycle repeats.

After the global system is solved, there is a check to see if the crack has grown, or if new adhesive failure has been detected. If this is the case, the sub-assembly is adjusted by changing the lengths of the sub-assembly elements, and the global system is re-solved. This is done until no new adhesive failure occurs and the crack is in equilibrium. A crack scaling constant, C_5, has been introduced to speed up or slow down crack growth as needed, and is used in the equation

$$l_{crack}^{cur} = l_{crack}^{cur} - C_5(l_{crack}^{cur} - l_{crack}^{prev}) \tag{11}$$

where l_{crack}^{prev} is the previous crack length (prior to the global Newton-Raphson procedure) and l_{crack}^{cur} is the current crack length. Setting $C_5 < 0$ causes the crack to grow further than detected, and is useful when multiple iterations are needed to find crack equilibrium. Setting $C_5 > 0$ causes the crack to grow less than detected, and is necessary when crack overshoot is a concern.

The advantage of this method is that fewer elements are needed in order to accurately capture crack growth. One can use the minimum elements needed to accurately capture the material and geometric nonlinear effects without crack growth being a factor. This can mean dramatically reducing the elements required, especially when there is little material nonlinearity and strains in the joint are small.

One of the major disadvantages of this method is the increased computational time. A local nonlinear problem must be solved within each iteration of the global nonlinear problem. Although the local nonlinear problem is always limited to three elements, it can significantly increase the runtime. Furthermore, the global load increment is repeated if the crack grows and the sub-assemblies need to be created or re-meshed. Although the crack scaling parameter can significantly help in limiting the iterations needed to find crack equilibrium this process can still be costly. However, the costs can be justified if joint strength prediction is of concern. Joint strength has been identified as a controlling factor in the ultimate load bearing capacity of many bonded structures.

Method

The aim of this study was to introduce the concept of adaptive shape functions and an internal adaptive mesh for the joint element and show how these methods can be used to reduce the amount of elements or integration points needed to reach a converged solution for the failure of adhesively bonded joints. To demonstrate the effect that these methods have, two sets of examples will be introduced. First, the bonded joint element model will be compared with and without adaptive mesh and adaptive shape functions to show when these methods are most effective at reducing computational time and how effective they can be. Second, the bonded joint element model is validated against a commercial CZM model and the computational times will be compared.

Joint Element Model Comparison

First, the bonded joint element model was used with and without adaptive shape functions (ASF) and adaptive mesh (AM) to see the effect of these methods. Four variations of the joint element model were compared (Table 1). The first one, standard joint elements, has no ASF or an AM. The shape functions are calculated based on the initial, undamaged state of the element. The adhesive is considered to be failed when the criterion is reached, and load carrying capability of the failed section of adhesive is set to zero in both shear and peel. The ASF model is the same as the standard model except with the shape functions being recalculated as the adhesive softens, and the AM model is the same as the standard model except that the failure of adhesive results in an introduction of internal nodes within the element and the position of these nodes changes as the crack in the adhesive grows. Finally, the last model, adaptive shape functions and mesh (ASF+M) combines both techniques.

Two different joints are analyzed, a double cantilever beam (DCB) and a single lap joint (see Figure 6(a) and (b), respectively). The DCB joint was selected because the crack typically grows progressively through the joint and the adhesive is loaded in mode I only. The single lap joint analyzed in this study results in catastrophic failures (no progressive failure) and mixed mode loading. The boundary conditions, loading and geometry of the two joints are shown in Figure 6.

For each joint configuration, two different adhesives are analyzed to show how effective adaptive shape functions and adaptive internal mesh methods are for highly plastic and brittle adhesives. The adhesives had an initial Young's modulus of 4 GPa, a maximum stress of 50 MPa, an initial shear modulus of 1.4 GPa, and a maximum shear stress of 29 MPa. The first adhesive displayed material nonlinearity only, and the stress-strain relationship was defined by a tanh function with the initial slope and maximum stress dictated by the aforementioned properties (see Figure 7(a)). There was no failure of the adhesive, it was allowed to strain indefinitely. This case is interesting because it reflects the global yielding failure theory introduced by Crocombe (Ref. 13), which states that the upper bound of the strength of a joint can be found by determining the point at which the whole adhesive layer has a tangent modulus of zero. The second adhesive used in the study had a linear stress-strain relationship up until failure (Figure 7(b)). As before, the slope of the stress-strain relationship was defined previously, along with the stress at failure.

TABLE 1.—FOUR JOINT ELEMENT MODEL
VARIATIONS COMPARED

Joint element model variation	Adaptive shape functions	Adaptive mesh
Standard	-	-
ASF	X	-
AM	-	X
ASF + M	X	X
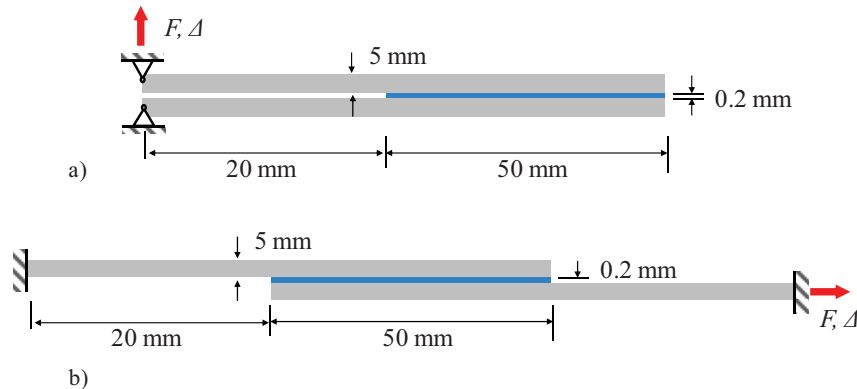
Figure 6.—Joint configurations used in the joint model comparison: (a) double cantilever beam (DCB) joint and (b) single lap joint (SLJ), where both joints are 20 mm wide (not to scale).
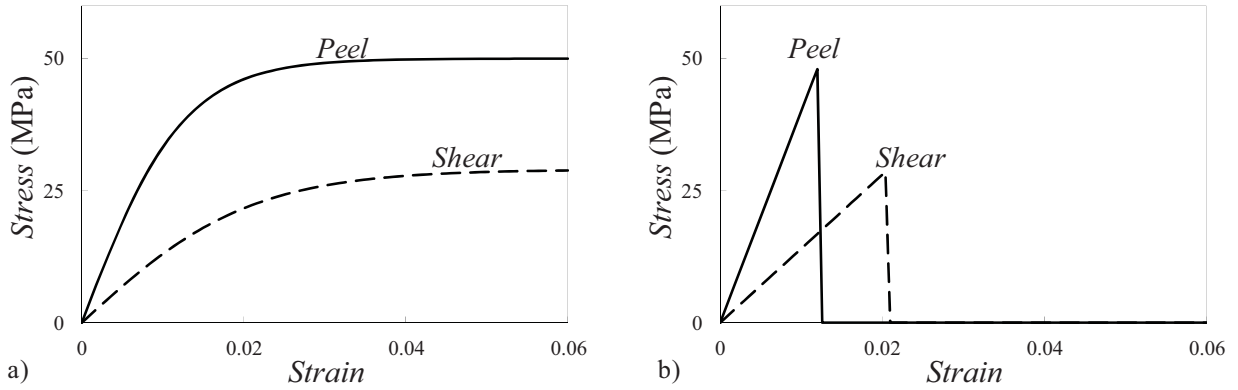
Figure 7.—Adhesive stress/strain relations used to demonstrate the convergence improvements using adaptive shape functions and adaptive mesh for adhesives displaying (a) material nonlinearity and (b) brittle material behavior.

Two values were compared between the variations of the model: integration points and computational time to convergence. Convergence is reached when the error of the analysis is less than 1 percent. The error is defined in one of two ways. For joint configurations which display progressive crack growth (i.e., DCB joint configuration with both adhesives and single lap joint with the adhesive with nonlinear material properties but no failure) the error, e_1, is defined as

$$e_1 = \frac{1}{N} \sum_{i=1}^{N} \frac{\left| F(\Delta_i) - F_\infty(\Delta_i) \right|}{F_\infty(\Delta_i)} 100 \tag{12}$$

where N is the number of load increments, $F(\Delta_i)$ is the end force at load increment i, and $F_\infty(\Delta_i)$ is the end force for the fully converged solution at load increment i. This is a measure of the average percent deviation of the load-displacement plot in the load-direction. When the joint fails catastrophically, or with no progressive crack growth, the error is taken as simply the percent deviation of the maximum load,

or

$$e_2 = \frac{\left| F_{max} - F_{max}^\infty \right|}{F_{max}^\infty} 100 \tag{13}$$

where e_2 is the error, F_{max} is the maximum load (i.e., strength) and F_{max}^∞ is the strength of the fully-converged solution. The analyses were all run on the same personal computer with 8 GB of RAM. While the actual computational time should be considered more of a qualitative property, the computational times of the different models relative to one another should be considered significant.

Finally, to identify circumstances under which using adaptive shape functions becomes highly advantageous, a single lap joint with an adhesive containing a trapezoidal stress-strain relation and different levels of strain energy before failure as shown in Figure 8 was analyzed. The initial slope and maximum stress of the stress-strain relation is the same as that defined for the previously studied adhesives and the final slope was a negative value of the initial slope. The total area under the curve, (W_{Ic} for mode I and W_{IIc} for mode II) was set as an integer multiple of the area the curve for the equivalent triangular stress-strain relation (W_{aI} for mode I and W_{aII} for mode II). Mode I and mode II strain energies were both increased, so that W_c/W_a represents the value of W_{Ic}/W_{aI} and W_{IIc}/W_{aII} simultaneously. AM and
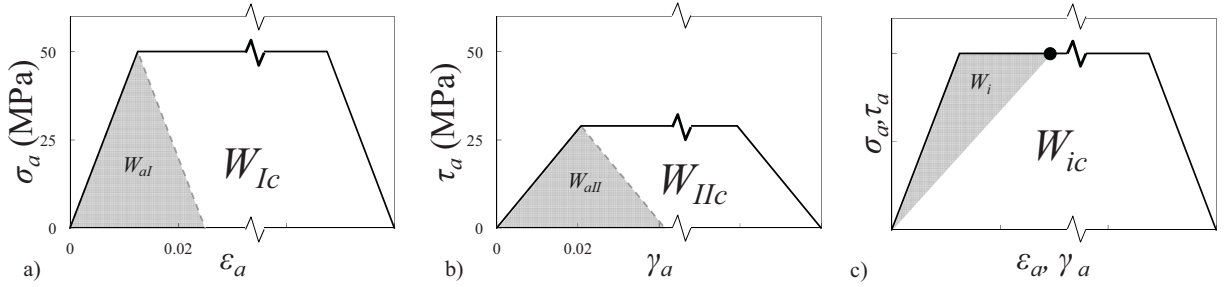
Figure 8.—Trapezoidal stress/strain relations for (a) normal and (b) shear used to show the benefits of using adaptive shape functions. The length of the horizontal region of the trapezoid was extended or shortened to get different W_o/W_a ratios. The current energy (c) defined for mode I and II.

ASF+M models were used, and computational time (t) and integration points (n) needed to reach convergence was compared in order to see how adaptive shape functions effects the computational time for adhesives with different amounts of critical strain energy.

The adhesive was defined as failed when the following relation was satisfied:

$$1 \leq \frac{W_I}{W_{Ic}} + \frac{W_{II}}{W_{IIc}} \qquad (14)$$

where W_I and W_{II} are defined as the current strain energy, as shown in Figure 8. It should be noted that this is synonymous to mixed-mode laws used for cohesive zone element models, except with fracture energy rather than strain energy. Since the adhesive of the joint element was assigned a thickness, we speak of everything in terms of stress/strain rather than traction/separation. However, since the displacements in the adhesive are assumed to be linear in the thickness direction of the adhesive, the fracture energy and separation can be obtained by simply scaling the strain energy and strain by the adhesive thickness. If the model is extended to include displacements of a higher order through the thickness, the traction/separation and stress/strain relations can no longer be linked. Therefore, we use the stress/strain relation for generality.

Comparison With Cohesive Zone Model

The joint element models were also compared to a cohesive zone model in Abaqus/Standard v6.11-1 finite element software (Ref. 7) using pre-existing modules within the software. The implicit, static finite element solver was used and a finite element mesh convergence study was performed to ensure numerical convergence was achieved. The adherends in the Abaqus models were discretized with 2D, linear, quadratic, plane strain, incompatible modes, CP4EI elements. These elements were chosen to better represent the linear bending action in the adherends. The adherends were assigned linear elastic material properties.

Cohesive elements (COH2D4) were used to represent the adhesive layers in the Abaqus models. These 2D elements were given a finite thickness according to the thickness of the adhesive and the constitutive response was governed using a traction-separation description. Element tractions are related to the nodal separation through a traction-separation law. Typically, the area under the traction-separation curve is equal to the fracture toughness of the material. For these analyses, a bi-linear traction-separation law was chosen. A simple, maximum stress criterion was used to mark the initiation of softening within the element, and the power law, mixed mode implementation within Abaqus was used to couple the opening and shear fracture modes. Both the Abaqus and joint models used the same adhesive strengths used in the earlier examples. The mode I and mode II fracture toughnesses employed in the Abaqus model were chosen such that they were equal to the critical strain energy densities, used in the joint models, scaled by the thickness of the adhesive ($G_{IC} = 625$ N/m, $G_{IIC} = 601$ N/mm).

The Abaqus built-in cohesive elements were considerably less flexible than the joint element, so the joint element failure criterion and constitutive relations were altered to match the cohesive elements. For the case of single mode loading (DCB: mode I only), the constitutive relation shown in Figure 9(a) was used for both models (except the cohesive zone model was scaled by the adhesive thickness to get a traction-separation law). The critical strain energies were the same as for the trapezoidal example when $W_{ia}/W_{ic} = 5$.

Since the joint element model considers the adhesive to be made of uncoupled shear and normal springs, the constitutive law had to be adjusted to give similar results to that of the cohesive element model for mixed-mode loading (SLJ). The built in cohesive zone model used a quadratic power law softening criterion, where softening was initiated when

$$\left(\frac{\sigma_a}{\sigma_{Ic}}\right)^2 + \left(\frac{\tau_a}{\tau_{IIc}}\right)^2 = 1 \tag{15}$$

To adapt the joint element constitutive relation to this softening criterion, the shear to peel ratio, ψ, was assumed to be constant throughout the loading and defined as

$$\psi = \frac{\sigma_{aMax}}{|\tau_{aMax}|} \tag{16}$$

where σ_{aMax} and τ_{aMax} were the maximum peel and shear stresses in the adhesive found through a linearly elastic analysis. Finally, using Equations (15) and (16), the adjusted peel and shear stresses at softening, σ_c and τ_c, were found using

$$\left(\frac{1}{\tilde{\tau}_{Ic}}\right)^2 = \left(\frac{\psi}{\sigma_{Ic}}\right)^2 + \left(\frac{1}{\tau_{IIc}}\right)^2 \text{ and } \tilde{\sigma}_{Ic} = \psi\tilde{\tau}_{IIc}. \tag{17}$$

For the cohesive zone model, the downward slopes for mode I and mode II are adjusted so that both modes reach zero traction when Equation (15) (peel and shear stress being replaced with mode I and mode II fracture energies) is satisfied, assuming that the ratio of peel to shear occurring at the onset of softening remains constant. For the joint element, this translates into cracking of the adhesive when:

$$\left(\frac{W_I}{W_{Ic}}\right)^2 + \left(\frac{W_{II}}{W_{IIc}}\right)^2 = 1 \tag{18}$$

Assuming the ratios of peel to shear stress and peel to shear strain remain constant, this yields the following adjusted critical strain energies:

$$\left(\frac{1}{\tilde{W}_{Ic}}\right) = \left(\frac{1}{W_{Ic}}\right)^2 + \left(\frac{E_a\psi^2}{G_aW_{IIc}}\right)^2 \text{ and } \tilde{W}_{IIc} = \tilde{W}_{Ic}\frac{G_a}{E_a\psi^2}. \tag{19}$$

These relation yields the mixed-mode adjusted constitutive relation shown in Figure 9(a).
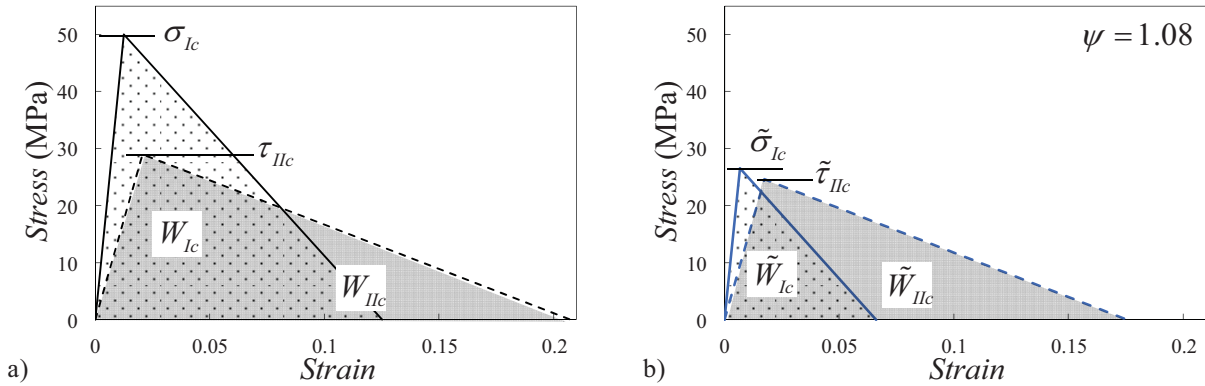
Figure 9.—Constitutive law joint element for comparison with cohesive elements, (a) with single-mode constitutive laws and (b) mixed-mode adjusted constitutive law for $\psi = 1.08$.

Results and Validation

Adaptive shape functions (ASF) and an adaptive internal mesh (AM) were introduced to the joint element to reduce the number of elements needed to capture adhesive nonlinearity and crack growth when modeling an adhesively bonded joint. The following section illustrates the benefit of these two methods in reducing computational time, elements required, and integration points required. The first section compares the joint element model with and without these features for different joint configurations and adhesive types, while the final section compares the model with a commercial code cohesive zone model.

Joint Element Model Comparison

Double Cantilever Beam (DCB)

The first joint configuration to be studied was the DCB configuration. For this configuration, the adhesive only experiences mode I loading and crack growth occurs in a progressive manner. This analysis is useful in showing how the different variations of the joint element model behave under progressive failure and crack growth. The number of elements, number of integration points, and computational time for both adhesives are shown in Table 3. Corresponding load versus displacement plots are shown in Figure 10. Since the failure is progressive and maximum load is only one integral part of the results, the error measurement e_1 is used and convergence occurs when the error falls below 1 percent.

The first adhesive considered was the ductile adhesive with no failure, but softening only. Since no crack forms for this adhesive, adaptive mesh is not needed and only standard elements and elements with adaptive shape functions are compared. The adaptive shape functions were extremely effective in reducing the number of integration points and computational time required to get a converged solution, with a computational time two orders of magnitude smaller. However, even using adaptive shape functions, the converged solution could not be captured with merely one element, but three were required.

The second adhesive considered was a brittle adhesive, with the stress-strain relation for mode I and mode II remaining linear until failure. The standard joint elements and adaptive shape function models both performed similarly, with similar computational times. However, the adaptive mesh method was pivotal in reducing the computational time significantly. Since there was no nonlinearity before failure in the adhesive, the adaptive shape functions did not affect the analysis except by adding to the computational time since the shape functions had to be recalculated at every load step.

TABLE 2.—COMPARISON OF NUMBER OF ELEMENTS (n_{el}), NUMBER OF INTEGRATIONS POINTS (n), AND COMPUTATIONAL TIME (t) FOR THE CONVERGED SOLUTION ($e_1 < 1$ PERCENT) FOR THE DCB JOINT WITH DIFFERENT MODELS AND ADHESIVES

Model	Ductile adhesive			Brittle adhesive		
	n_{el}	n	t (sec)	n_{el}	n	t (sec)
Standard joint elements	40	680	4435	40	680	1988
Adaptive shape functions (ASF)	3	25	71	1	1025	1498
Adaptive mesh (AM)	----	----	----	1	65	33
ASF + M	----	----	----	1	65	112
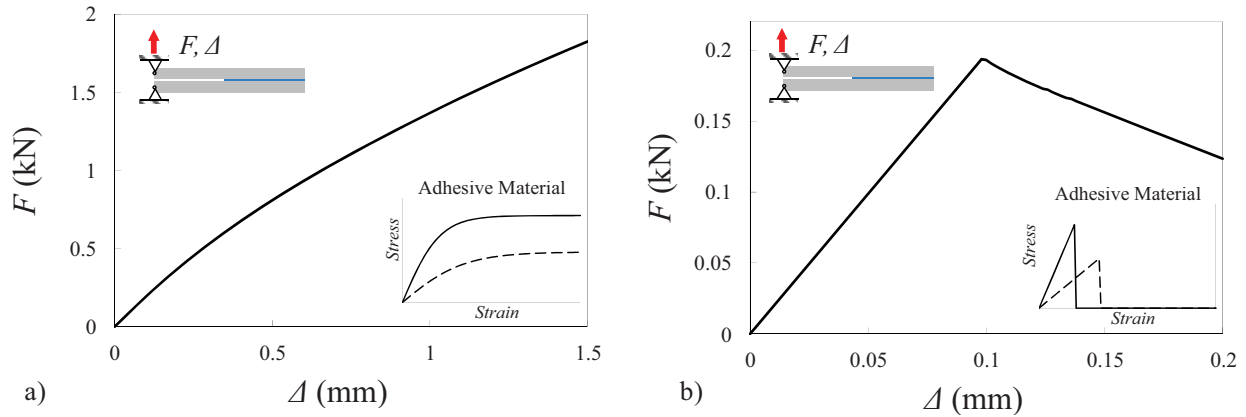
Figure 10.—DCB joint configuration with load versus displacement plot for the models with (a) a ductile and (b) a brittle adhesive.

Single Lap Joint (SLJ)

The single lap joint was the next joint configuration to be considered, which is a more realistic joining configuration containing mode I and mode II loading in the adhesive, and catastrophic crack growth rather than progressive crack growth, except for the case of the nonlinear adhesive with no failure. When catastrophic failure occurred, it was more practical to use the error value e_2, since it deals with the maximum load only. The number of elements, number of integration points, and computational time for both adhesives are shown in Table 3. Corresponding load versus displacement plots are shown in Figure 11.

The first adhesive considered for the single lap joint configuration was the nonlinear adhesive with no failure. The maximum load is reached when the adhesive becomes fully softened in shear (the tangent shear modulus is nearly zero along the entire length of the adhesive). Similar to the DCB configuration, models with adaptive mesh were not considered because no crack growth modeling was required. As can be seen, using adaptive shape functions for this case made a huge difference, with two orders of magnitude less integration points required and three orders of magnitude faster analysis. Obviously, for this case, it would be highly advantageous to use adaptive shape functions.

The second adhesive considered for the single lap joint was the brittle adhesive, which is linear until failure. As with the DCB configuration with the same adhesive, adaptive shape functions are not helpful because the adhesive has no nonlinearity, so recalculating the shape functions at every step is unnecessary. However, the adaptive mesh model was extremely fast for this configuration. Since the adhesive stress-strain relation was linear, the solution could be found in one Newton-Raphson iteration, with the internal mesh creation only adding a small amount of additional time.

TABLE 3.—COMPARISON OF NUMBER OF ELEMENTS (n_{el}), NUMBER OF INTEGRATIONS POINTS (n),
AND COMPUTATIONAL TIME (t) FOR THE CONVERGED SOLUTION ($e_1/e_2 < 1$ PERCENT) FOR THE
SLJ JOINT WITH DIFFERENT MODELS AND ADHESIVES

Model	Ductile adhesive			Brittle adhesive		
	n_{el}	n	t (sec)	n_{el}	n	t (sec)
Standard joint elements	80	1360	35255	40	680	11521
Adaptive shape functions (ASF)	2	10	71	40	680	12364
Adaptive mesh (AM)	--	----	-------	1	33	2
ASF + M	--	----	-------	1	33	25
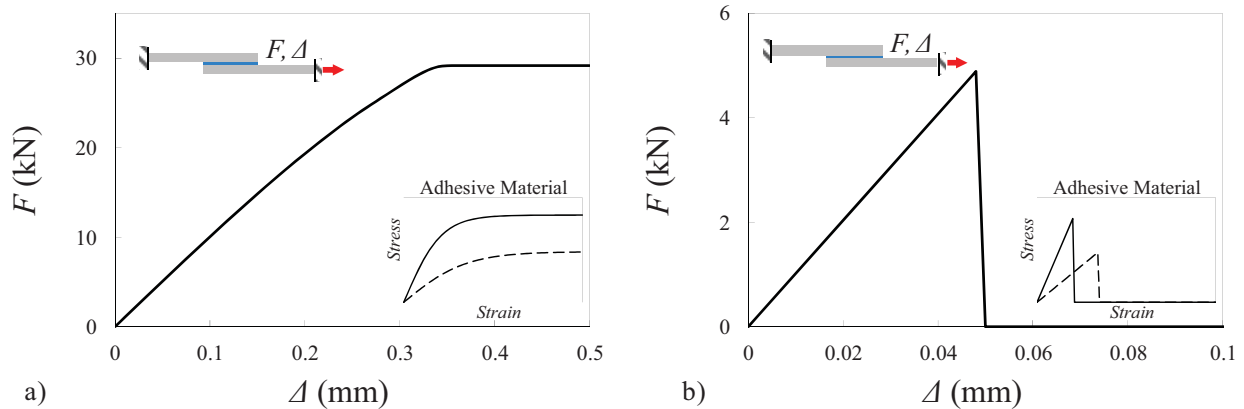
Figure 11.—SLJ joint configuration with load versus displacement plot for the models with (a) a ductile and (b) a brittle adhesive.

Trapezoidal Adhesive With Variable W

Considering the foregoing results, one can hypothesize that the additional cost of calculating the adaptive shape functions at every load step is beneficial for adhesives with high fracture toughness. To further investigate this hypothesis, the adaptive mesh model was compared with and without adaptive shape functions for an adhesive with a trapezoidal stress-strain relation and variable amounts critical strain energy W, which in this study is synonymous with the fracture toughness normalized by the adhesive layer thickness. The strain energy for each mode (W_{Ic} and W_{IIc}) is normalized by the strain energy of an adhesive with a triangular stress-strain relation with the same critical stress and slopes. The computational times (t) and integration points (n) needed for a converged solution ($e_2 < 1$ percent) for the two models are compared in Figure 12.

In Figure 12 the computational time and integration points for the converged solution of the adaptive mesh model is normalized by that of the adaptive shape function + adaptive mesh model. For values of $\bar{t} > 1$, the ASF+M model is faster than the AM model. The same can be said about integration points, $\bar{n}$. This plot shows that for low W_c values ($W_c/W_a < 3$), it is not advantageous to use the adaptive shape functions. The two models appear to have similar results for $W_c/W_a = 3$, and for $W_c/W_a > 3$ using adaptive shape functions improves both the computational time and number of integration points needed. For $W_c/W_a = 7$, the converged solution was reached with the aid of adaptive shape functions in 1/30th the computational time. It is expected that the time savings would continue to increase with an increase in W_c. With increasing toughness of modern aerospace grade adhesives, it is expected that adaptive shape functions would be beneficial for many, if not most, adhesive bonding configurations.
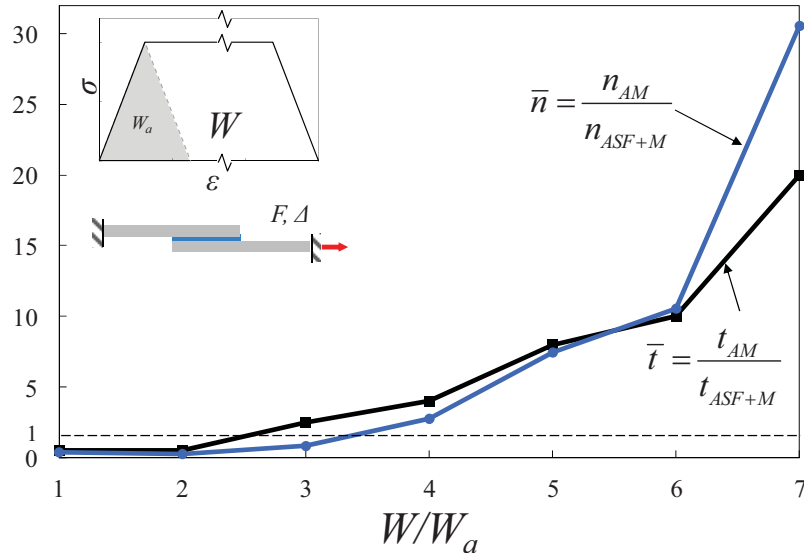
Figure 12.—Comparison of the computational time (t) and integration points (n) needed to reach convergence ($e_2 < 1$ percent) for the joint element model with adaptive mesh (AM) and with both adaptive mesh and adaptive shape functions (ASF+M) for different stress/strain relations.

Comparison With Cohesive Zone Model

In order to compare the joint element model with more standard adhesive joint finite element techniques, a DCB and SLJ were modeled using the cohesive zone elements in Abaqus and the joint element models (ASF+M and AM). The coarsest finite element meshes for the Abaqus model and the ASF+M model are shown in Figure 13 for both joint configurations. The meshes shown represent the coarsest meshes that provided a converged solution ($e_1/e_2 < 1$ percent). Both Abaqus models contained 2800 elastic, CPE4I elements, and 100 COH2D4 cohesive zone elements. The number of elements, number of integration points, and computational time for both adhesives are shown in Table 4, and the corresponding load versus displacement plots are shown in Figure 14. Computational time was not explicitly compared because the vast difference between an optimized commercial code and a flexible research code does not provide for a good comparison. However, the number of elements and total number of integration points should provide a good comparison. Since both joint configurations with the aforementioned adhesive had significant nonlinearity and adhesive cracking, both the adaptive shape functions (ASF) and adaptive mesh (AM) were beneficial in providing a converged solution with a minimum number of elements.

When considering the adaptive shape functions, one might conclude that with enough integration points, the nonlinearity of any adhesive could be captured with one element. This may be true in theory, but numerical stability issues caused a requirement of more elements. With very long elements and highly non-linear tangent stiffness (especially negative stiffness), the chances increase that the matrix exponential used to solve Equation (10) becomes unstable and does not converge at large values of x. Therefore, more elements are needed to shorten the shape functions and keep them in the stable regime. Future work will include applying improved matrix exponential solution procedures to correct this problem.
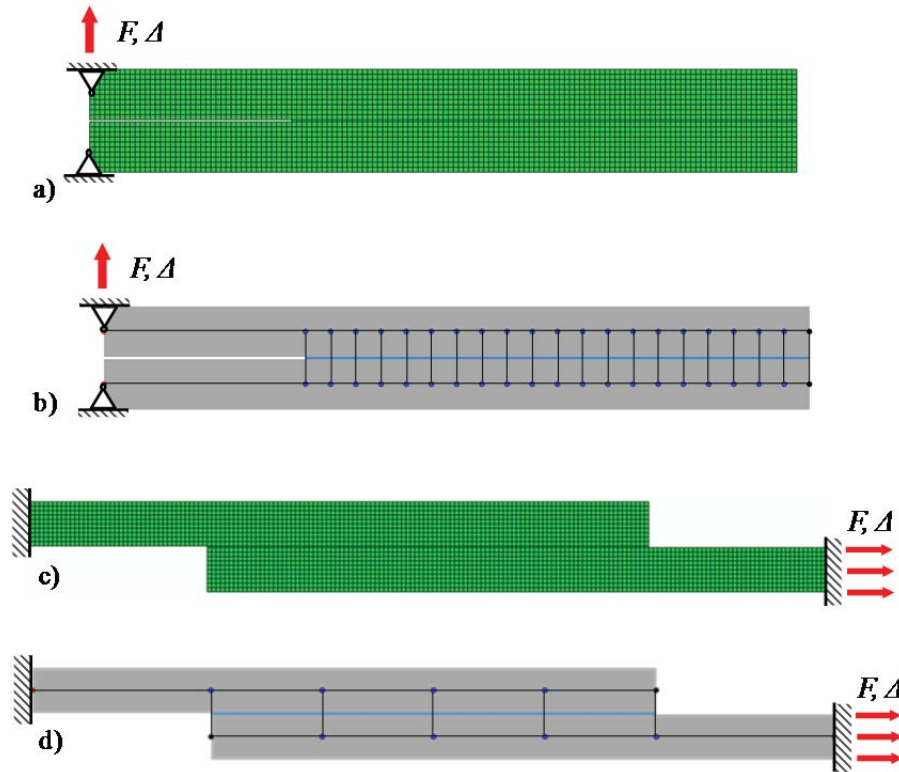
Figure 13.—Mesh used for the DCB (a, b) and SLJ (c, d) configurations for the Abaqus finite element simulations (a, c) and the ASF+M model (b, d).

TABLE 4.—COMPARISON OF NUMBER OF ELEMENTS (n_{el}), NUMBER OF INTEGRATIONS POINTS (n), AND COMPUTATIONAL TIME (t) FOR THE CONVERGED SOLUTION ($e_1/e_2 < 1$ PERCENT) FOR THE JOINTS WITH DIFFERENT MODELS

Model	Double cantilever beam		Single lap joint	
	n_{el}	n	n_{el}	n
Adaptive mesh (AM)	320	5440	160	1360
ASF + M	20	340	4	51
Abaqus	2800	11400	2800	11400
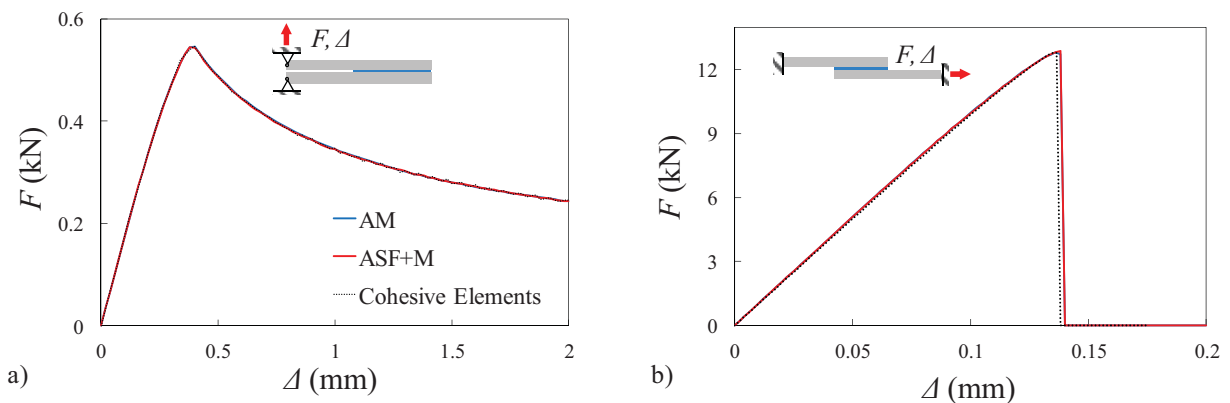
Figure 14.—Comparison of load versus displacement plots of different models for (a) DCB and (b) SLJ configurations.

Summary and Conclusions

This study deals with semi-analytical finite elements with shape functions which are *determined* based on a model rather than *prescribed*, specifically bonded joint finite elements. Two methods were demonstrated to decrease the number of elements needed for a converged answer.

The first is adaptive shape functions (ASF). Since the shape functions are determined from a model, the material properties are an input parameter affecting the shape functions directly. When the material softens, i.e., the material properties change, the shape functions can be updated based on the new softened properties. This causes the shape functions to adapt to the material, making them very representative of the actual structural behavior and allowing a single element to remain accurate even with highly nonlinear materials.

The second method for decreasing the number of elements needed was using an adaptive internal mesh (AM). When a portion of adhesive was cracked within a joint element, the joint element was re-meshed with beam elements and a joint element. This re-meshing occurred internally within the element, requiring no alteration of the global model. This method can capture progressive failure of an adhesive with very few elements, but requires a nonlinear finite element model to be solved within cracked element.

Joint element models with and without the two methods were compared with each other for a double cantilever beam and single lap joint configuration with brittle and ductile adhesives. It was shown that the adaptive shape function method became more beneficial with increasing ductility of the adhesive. With sufficient ductility, the time spent to recalculate the shape functions at every load increment became insignificant when compared to the reduction in mesh and integration points. The adaptive mesh method was beneficial for all cases with progressive and catastrophic material cracking.

Finally, the joint element model with both methods was compared with a standard, built-in cohesive zone model in Abaqus. Using both adaptive shape functions and mesh, less than 3 percent of the elements and integration points were needed, which is a significant gain.

Both methods have potential for broader applications within finite elements. The adaptive shape functions concept can be utilized whenever the shape functions have some sort of material or geometrical parameter with them to improve the accuracy of shape functions during changes in materials and geometry. Furthermore, the adaptive internal mesh can and has been used to capture the introduction and propagation of discontinuities within an element without requiring a global re-meshing of the model.

References

1. Hart-Smith L. Adhesive Bonding of Composite Structures—Progress to Date and Some Remaining Challenges. Journal of Composites Technology and Research 2002;24(3):133.
2. Samantha Bell. Structural adhesives deliver lighter composite structures with performance and costs benefits. Reinforced Plastics 2012.
3. Volkersen O. Die Nietkraftverteilung in Zugbeanspruchten mit Konstanten Laschenquerschritten. Luftfahrtforschung 1938;15:41–47.
4. Goland, Reissner E. The stresses in cemented joints. Journal of Applied Mechanics 1944;11:A17–A27.
5. Hart-Smith LJ. Adhesive-bonded double-lap joints. NASA CR-112235 1973.
6. Hart-Smith LJ. Adhesive-bonded single-lap joints. NASA CR-112236 1973:116.
7. Delale F, Erdogan F, Aydinoglu M n. Stresses in Adhesively Bonded Joints: A Closed-Form Solution. Journal of Composite Materials 1981;15(3):249–271.
8. Mortensen F, Thomsen OT. Analysis of adhesive bonded joints: a unified approach. Composites Science and Technology 2002;62(7–8):1011–1031.
9. Frostig Y, Thomsen OT, Mortensen F. Analysis of Adhesive-Bonded Joints, Square-End, and Spew-Fillet—High-Order Theory Approach. Journal of Engineering Mechanics 1999;125(11):1298–1307.

10. Tsai MY, Morton J. An evaluation of analytical and numerical solutions to the single-lap joint. International Journal of Solids and Structures 1994;31(18):2537–2563.
11. Adams RD, Peppiatt NA. Stress Analysis of Adhesive Bonded Tubular Lap Joints. The Journal of Adhesion 1977;9(1):1–18.
12. Tsai MY, Oplinger DW, Morton J. Improved theoretical solutions for adhesive lap joints. International Journal of Solids and Structures 1998;35(12):1163–1185.
13. Crocombe AD. Global yielding as a failure criterion for bonded joints. International Journal of Adhesion and Adhesives 1989;9(3):145–153.
14. Harris JA, Adams RA. Strength prediction of bonded single lap joints by non-linear finite element methods. International Journal of Adhesion and Adhesives 1984;4(2):65–78.
15. Bednarcyk B, Bansal Y, Collier C, Pindera M-J, Zhang J. Analysis Tools for Adhesively Bonded Composite Joints, Part 1: Higher-Order Theory. AIAA Journal 2006;44(1):171–180.
16. Zhang J, Bednarcyk BA, Collier C, et al. Analysis Tools for Adhesively Bonded Composite Joints, Part 2: Unified Analytical Theory. AIAA Journal 2006;44(8):1709–1719.
17. Zhang J, Bednarcyk B, Collier C, et al. 3D stress analysis of adhesively bonded composite joints. InVol 4.; 2005:2750–2773.
18. Camanho PP, Tong L. Composite joints and connections: Principles, modelling and testing. Woodhead Publishing; 2011, 544 p.
19. Towse A, Potter KD, Wisnom MR, Adams RD. The sensitivity of a Weibull failure criterion to singularity strength and local geometry variations. International Journal of Adhesion and Adhesives 1999;19(1):71–82.
20. Ortiz M, Pandolfi A. Finite-deformation irreversible cohesive elements for three-dimensional crack-propagation analysis. International Journal for Numerical Methods in Engineering 1999;44(9):1267–1282.
21. Camanho PP, Dávila CG. Mixed-Mode Decohesion Finite Elements for the Simulation of Delamination in Composite Materials. Hampton, Virginia: Langley Research Center; 2002.
22. Krueger R. Virtual crack closure technique: History, approach, and applications. Appl. Mech. Rev. 2004;57(2):109–143.
23. Xie D, Waas AM. Discrete cohesive zone model for mixed-mode fracture using finite element analysis. Engineering Fracture Mechanics 2006;73(13):1783–1796.
24. Goutianos S, Sørensen BF. Path dependence of truss-like mixed mode cohesive laws. Engineering Fracture Mechanics 2012;91:117–132.
25. Guiamatsia I, Ankersen JK, Davies GAO, Iannucci L. Decohesion finite element with enriched basis functions for delamination. Composites Science and Technology 2009;69(15–16):2616–2624.
26. Guiamatsia I, Davies GAO, Ankersen JK, Iannucci L. A framework for cohesive element enrichment. Composite Structures 2010;92(2):454–459.
27. Ostergaard MG, Ibbotson AR, Roux OL, Prior AM. Virtual testing of aircraft structures. CEAS Aeronautical Journal 2011;1(1-4):83–103.
28. Eisenberger M, Yankelevsky DZ. Exact stiffness matrix for beams on elastic foundation. Computers & Structures 1985;21(6):1355–1359.
29. Aydoğan M. Stiffness-Matrix Formulation of Beams with Shear Effect on Elastic Foundation. Journal of Structural Engineering 1995;121(9):1265–1270.
30. Gustafson PA, Waas AM. A bonded joint finite element for a symmetric double lap joint subjected to mechanical and thermal loads. International Journal for Numerical Methods in Engineering 2009;79(1):94–126.
31. tapleton SE, Waas AM. Reduced-order Modeling Of Adhesively Bonded Joints Using An Enhanced Joint Finite Element. In Proceedings of the 52nd International SAMPE Symposium. Salt Lake City, UT; 2010.
32. Stapleton SE, Waas AM, Arnold SM. Functionally graded adhesives for composite joints. International Journal of Adhesion and Adhesives 2012;35:36–49.

33. Stapleton SE, Waas A. Macroscopic Finite Element for a Single Lap Joint. In AIAA/ASME/ASCE/AHS/ASC 50th SDM Conference. Palm Springs, California; 2009.
34. Rudraraju S, Salvi A, Garikipati K, Waas AM. Predictions of crack propagation using a variational multiscale approach and its application to fracture in laminated fiber reinforced composites. Composite Structures 2012;94(11):3336–3346.
35. Rudraraju S, Salvi A, Garikipati K, Waas AM. Experimental observations and numerical simulations of curved crack propagation in laminated fiber composites. Composites Science and Technology 2012;72(10):1064–1074.
36. Scott E. Stapleton, Anthony M. Waas. The Analysis of Adhesively Bonded Advanced Composite Joints Using Joint Finite Elements. Cleveland, OH: NASA Glenn Research Center; 2012.
37. Belytschko T, Hsieh BJ. Non-linear transient finite element analysis with convected co-ordinates. International Journal for Numerical Methods in Engineering 1973;7(3):255–271.
38. Crisfield MA. Non-Linear Finite Element Analysis of Solids and Structures. Wiley; 1996, 362 p.
39. Crisfield MA, Moita GF. A unified co-rotational framework for solids, shells and beams. International Journal of Solids and Structures 1996;33(20–22):2969–2992.
40. Guyan RJ. Reduction of stiffness and mass matrices. AIAA Journal 1965;3(2):380–380.
41. Chen S, Pan HH. Guyan reduction. Communications in Applied Numerical Methods 1988;4(4):549–556.
42. Chandrupatla TR, Belegundu AD. Introduction to Finite Elements in Engineering. 2 Har/Dsk. Prentice Hall College Div; 1996,461 p.